Type I interferon drives a cellular state inert to TCR-stimulation and could impede effective T-cell differentiation in cancer

Dillon Corvino[1*], Martin Batstone[2,3], Brett G.M Hughes[2,3], Tim Kempchen[1], Susanna S Ng[1], Nazhifah Salim[1], Franziska Schneppenheim[1], Denise Rommel[1], Ananthi Kumar[1], Sally Pearson[4], Jason Madore[4], Lambross T. Koufariotis[4], Lisa Maria Steinheuer[1], Dilan Pathirana[5], Kevin Thurley[1], Michael Hölzel[1], Nicholas Borcherding[6], Matthias Braun[7#], and Tobias Bald[1*#]

[1]Tumor-Immunobiology, Institute for Experimental Oncology, University Hospital Bonn, Bonn, Germany

[2]Royal Brisbane and Women's Hospital, Brisbane, Queensland, Australia

[3]Faculty of Medicine, University of Queensland, Brisbane, Queensland, Australia

[4]QIMR Berghofer Medical Research Institute, Herston, Australia

[5]Faculty of Mathematics and Natural Sciences, and the Life and Medical Sciences Institute (LIMES), Rheinische Friedrich-Wilhelms-Universität Bonn, Bonn, Germany

[6]Department of Pathology and Immunology, Washington University School of Medicine, St. Louis, MO, USA

[7]Department of Paediatric Haematology, Oncology and Immunodeficiency, Justus-Liebig-University Giessen, Giessen, Germany

Shared senior authorship

***Correspondence:**

Dillon Corvino, Institute for Experimental Oncology, University Hospital Bonn, Venusberg-Campus 1, 53127 Bonn, Germany; Corvino.Dillon@ukbonn.de

Tobias Bald, Institute for Experimental Oncology, University Hospital Bonn, Venusberg-Campus 1, 53127 Bonn, Germany; Tobias.Bald@ukbonn.de

Keywords: HNSCC TILs, scRNAseq, Type I IFN (ISG), CD8+ T-cells, GZMK expressing cells.

Abstract

Head and neck squamous cell carcinoma (HNSCC) arises from the mucosal epithelium of the oral cavity, pharynx, or larynx and is linked to exposure to classical carcinogens and human papillomavirus (HPV) infection. Due to molecular, immunological, and clinical disparities between HPV+ and HPV- HNSCC, they are recognized as distinct cancer types. While immune checkpoint inhibition (ICI) has demonstrated efficacy in recurrent/metastatic HNSCC, response variability persists irrespective of HPV status. To gain insights into the CD8+ T-cell landscape of HPV- HNSCC, we performed multimodal sequencing (RNA and TCR) of CD8+ tumor-infiltrating lymphocytes (TILs) from treatment-naïve HPV- HNSCC patients. Additionally, we subjected cells to *ex vivo* TCR-stimulation, facilitating the tracing of clonal transcriptomic responses. Our analysis revealed a subset of CD8+ TILs highly enriched for interferon-stimulated genes (ISG), which were found to be clonally related to a subset of granzyme K (GZMK)-expressing cells. Trajectory inference suggests ISG transition via GZMK cells towards terminal effector states. However, unlike GZMK cells, which rapidly an effector-like phenotype in response to TCR stimulation, ISG cells remain transcriptionally inert. Consequently, ISG cells may impede effective T-cell differentiation within the TME. Although, the functional consequences of ISG cells are poorly understood, we revealed that they possess receptors and ligands enabling cell-cell communication networks with key TME immunomodulators such as dendritic cells. Additionally, ISG cells were found to be a core feature across various tumor entities and were specifically enriched within tumor tissue. Thus, our findings illuminate the complexity of T-cell heterogeneity in HPV- HNSCC and reveal an overlooked population of IFN-stimulated CD8+ TILs. Further exploration of their functional significance may offer insights into therapeutic strategies for HPV- HNSCC and other cancer types.

Background

Head and neck squamous cell carcinoma (HNSCC) encompass cancers originating from the mucosal epithelium of the oral cavity, pharynx, or larynx. HNSCC is closely associated with myriad environmental and lifestyle factors such as air pollutants, tobacco, and alcohol consumption (Johnson et al. 2020). In addition, viral co-infection with human papillomavirus (HPV) is observed in a subset of HNSCC (~32%) patients (Ndiaye et al. 2014). Interestingly, HPV+ HNSCC is associated with more favourable prognosis especially in early stage disease (Fung et al. 2017; Lassen et al. 2009; Ang et al. 2010). The clinical benefit of HPV status is thought to derive from HPV-specific immune responses and the intrinsic immunogenicity of HPV (Nelson et al. 2017; Andersen et al. 2014).

Standard-of-care treatment options for HNSCC include surgical resection, radiotherapy, and chemotherapy (Johnson et al. 2020). However, immunotherapy-based treatment approaches such as immune checkpoint inhibition (ICI), have shown significant clinical benefit in the recurrent/metastatic setting (Vos et al. 2021). In fact, immune checkpoint inhibition has been approved for first-line treatment of patients with recurrent/metastatic (R/M) HNSCC (Burtness et al. 2019). Unfortunately, response to immunotherapy varies significantly. Variable responses may, in part, be attributed to the immunosuppressive tumor-microenvironment (TME) commonly observed in HNSCC (Johnson et al. 2020). While it is generally accepted that HPV+ HNSCC shows more robust anti-tumor immune responses compared to HPV− HNSCC, recent immunotherapy trials did not find an association between HPV status and response (Sacco et al. 2021; Ferris et al. 2016). Given, that CD8+ T-cells are recognized as key drivers of anti-tumoral responses, a better understanding of the CD8+ tumor-infiltrating lymphocyte (TIL) heterogeneity in HPV- patients is needed to improve the treatment for this subgroup of HNSCC.

Interferons (IFNs) are pleiotropic cytokines primarily produced by immune and stromal cells in response to pathogens or malignant transformation. Three types of IFNs have been described, which differ by the distinct receptors they bind and the subsequent signaling cascades induced. Type I IFNs (IFN-I) have well described roles in both anti-viral and anti-tumor responses. In particular, IFN-I can directly inhibit tumor growth by inhibiting proliferation and inducing apoptosis. In addition, IFN-I can act indirectly to induce anti-tumor immune responses,

for example via the activation of dendritic cells, natural killer cells or neutrophils (Bald et al. 2014). Simultaneously, IFN-I can reduce the pro-tumorigenic functions of regulatory T-cells and myeloid-derived suppressor cells (Yu, Zhu, and Chen 2022). In fact, IFN-I signaling is considered as a "third signal" of activation and important for naïve T-cell priming, activation, proliferation, and memory differentiation (Curtsinger and Mescher 2010). Thus, IFN-I is regarded as a crucial cytokine in facilitating cancer immunosurveillance and boosting the efficacy of cancer immunotherapies (Yu, Zhu, and Chen 2022; Fuertes et al. 2011; Diamond et al. 2011; Ruotsalainen et al. 2021). However, we have previously shown via genetic ablation, that IFN-I signaling is dispensable for the expansion and function of adoptively transferred tumor-specific CD8+ T-cells (Ruotsalainen et al. 2021). In addition, several studies also provide evidence that IFN-I signaling, at least in the later stages of anti-tumor immune responses, can promote pro-tumor changes and ultimately immune escape (Zhou et al. 2020). For example, IFN-I signaling is linked to expression of immune checkpoints, IL-10, Nos2 and the development of a T-cell exhaustion phenotype (Ruotsalainen et al. 2021; Chen et al. 2022; Sumida et al. 2022). Therefore, the effect of IFN-I signaling in the functional outcomes of tumor-infiltrating T-cells is multifaceted and requires further investigation.

Single-cell RNA sequencing (scRNA-seq) of immune cell subsets in cancer patients has enabled the high-resolution mapping of cellular heterogeneity. This methodology has been applied to the analysis of human T-cells in response to cancer immunotherapies (Sade-Feldman et al. 2018). However, traditionally this approach only focuses on assessing the transcriptional state of *ex vivo* isolated cells. Thus, capturing a snapshot of cellular transcriptomic landscape within the TME. Therefore, we leveraged an *ex vivo* perturbation via a short-term T-cell receptor (TCR) stimulation. Coupled with scRNAseq and single-cell TCR sequencing, we were able to study the clonal dynamics and evaluate the responsive potential of CD8+ tumor-infiltrating lymphocyte (TIL) subsets.

Herein, we sequenced over 11,000 resting and stimulated CD8+ TILs isolated from treatment-naïve HPV- HNSCC patients. As such, we were able to define *ex vivo* cellular states and their stimulation outcomes. Importantly, we identified a population of T-cells rich in IFN-stimulated genes (ISG). These ISG cells were found to be associated with an IFN-I signature and were specifically enriched within the tumor tissue of various tumor entities. Furthermore, these

cells were found to be clonally related to a population of cells highly expressing granzyme K (GzmK). However, unlike the GzmK subset, ISG-cells were transcriptionally inert to stimulation and thus possibly possess a unique role within the TME. This study sheds light on the existence of this overlooked population and begins to investigate their functionality.

Results

Single-cell RNA sequencing of CD8+ TILs from treatment-naive HNSCC patients identifies exhausted and effector populations

CD8+ T-cells are key drivers of anti-tumor responses. However, there is substantial heterogeneity in CD8+ T-cell phenotypes within TIL populations. As such, we sought to explore the diversity of CD8+ TILs in HPV- treatment-naïve non-R/M HNSCC patients. We isolated live CD45+CD3+CD4-CD8+ from 8 patients using flow cytometry-based cell sorting and subjected half of those cells to *ex vivo* CD3/28 TCR stimulation. After 5 hours of stimulation, we performed single-cell RNA and TCR sequencing to simultaneously identify CD8+ TIL phenotypes and clonotypes. We thereby were able to profile transcriptional changes in response to TCR-based stimulation (Figure 1A).

Sequencing data from both unstimulated and TCR-stimulated samples were integrated and projected onto a unified UMAP space (Figure 1B). This resulted in 14 distinct clusters of CD8+ TILs with the majority of identified clusters evenly distributed across both unstimulated and stimulated conditions (Supplementary Figure 1A). Importantly, two new clusters emerged specifically post-TCR-stimulation (clusters Stimulated-1; Stim-1 and Stimulated-Exhausted; $Stim_{EX}$). Three naïve/memory cell clusters were identified and annotated based on their expression of markers such as *IL7R*, *CCR7*, and *SELL* (Figure 1C). A cluster of cells expressing *GZMK* as well as *EOMES*, *NKG7*, *TNFRSF18* (encodes for GITR), and *CD69* was also identified (Figure 1D and data not shown). Additionally, a cluster of cells expressing high levels of various interferon-stimulated genes, including *ISG15*, *IFI6*, *IFIT3*, *MX1*, *ISG20*, *IFITM1*, *IFIT1*, *MX2*, and *OAS3* (Supplementary Figure 1B and data not shown) was recognized and annotated as the interferon-gene stimulated (ISG) cluster of cells (Figure 1D). The stimulated-1 (Stim-1) cluster from TCR-stimulated cells was enriched for the expression of immune effector molecules such as *IFNG*, *XCL1*, *XCL2*, *CRTAM*, *TNF*, *TNFSF14* (encodes for LIGHT) and

TNFRSF9 (encodes for 4-1BB) (Figure 1D and Supplementary figure 1B). Three exhausted cell clusters were also identified, all expressing high levels of canonical exhaustion markers such as, *TOX*, *HAVCR2*, *PDCD1* (encodes for Tim-3 and PD-1, respectively), *CTLA4*, *ENTPD1* (encodes CD39), and *TIGIT* (Figure 1E and Supplementary Figure 1B). One of these exhausted clusters was exclusively found post-TCR-stimulation and as such was designated as the Stimulated-Exhausted ($Stim_{EX}$) cluster. A small cluster of tissue-resident memory (TRM) cells was identified based on the expression of canonical TRM markers such as *ZNF683* (encodes for HOBIT), *PRDM1* (encodes for BLIMP1), *ITGA1* (encodes for CD49A), *ITGAE* (encodes for CD103), and *CXCR6* (Figure 1F and supplementary figure 1B). A small population of proliferating cells was also identified by their enrichment for proliferation and cell cycle genes, notably *MKI67* (encodes for Ki-67) (Figure 1F).

HNSCC TME is populated with unconventional CD8+ T-cells

We also identified three clusters of unconventional T-cells (Figure 1G and Supplementary Figure 1C). Two of these had gene expression patterns indicative of gamma delta (□δ) T-cell subsets. The third cluster expressed markers corresponding with a mucosal-associated invariant T (MAIT) cell population. □δ T-cell clusters could be differentiated based on the expression of TCR genes (Supplementary Figure 1D), marking the two clusters as the V□9Vδ2 T-cells (G9D2) and non-G9D2 populations. All unconventional T-cell populations expressed high levels of *CD3* and *CD8* as previously described (Kalyan and Kabelitz 2013; Gherardin et al. 2018) (Supplementary Figure 1E). Differential gene expression revealed that the G9D2 population expressed cytotoxicity markers such as *GZMA*, *GZMB*, *GZMH*, *GNLY*, *PRF1*, and *NKG7* (Supplementary Figure 1B and 1F). Non-G9D2 γδ T-cells expressed markers such as *TCF7*, *CD27*, *KLRD1*, and *SELL*. Analysis of differentially expressed transcription factors revealed that these three cell clusters had distinct and unique transcriptional regulatory programs (Supplementary Figure 1G). For example, G9D2 cells revealed specific enrichment for transcription factors *EOMES*, *ZEB2*, and *ZNF683* (encodes for HOBIT), while non-G9D2 cells were enriched for *ID3*, *IKZF2*, *TCF7*, and *BACH2*. Meanwhile, MAIT-cells demonstrated a distinct pattern of enrichment for transcription factors associated with the MAIT lineage, such as *RORA*, and *ZBTB16* (encodes for PLZF). Altogether, the unconventional T-cells, TRMs, and proliferative cells, cumulatively represented about ~10% of TILs within the dataset (Figure 1H).

Ex vivo TCR stimulation leads to the emergence of two transcriptionally distinct T-cell clusters

For further analysis, we removed the three unconventional T-cell clusters from the dataset and recalculated the UMAP coordinates (Figure 2A). We next sought to investigate the two cell clusters which predominantly arose from TCR-based stimulation. Importantly, both stimulation-induced clusters shared expression of a number of genes expected following TCR activation, including critical effector molecules such as *IFNG*, *GZMB* or *FASLG*, as well as activation markers as *ICOS* and *TNFRSF9* (encodes for 4-1BB) (Figure 2B). However, despite an overlap of activation-induced transcription, both stimulation-induced clusters showed distinct patterns of gene expression reminiscent of their origin (Figure 2C). For example, the Stim-1 cluster was enriched for genes such as *IL7R*, *XCL1*, *CD69*, *TNFSF14* (encodes for LIGHT), *CD28*, and *LTB*, whereas the $Stim_{EX}$ cluster expressed high levels of exhaustion markers such as *TOX*, *LAG3*, *HAVCR2* (encodes for TIM-3) and *CD96*. These basal gene expression profiles seem to overlap with gene expression of other clusters of the dataset. For example, genes enriched in Stim-1 cluster were also highly abundant in Naïve/memory, GZMK, and ISG clusters, while genes expressed within the $Stim_{EX}$ cluster were found enriched within the remaining two T_{EX} clusters and to a lesser extend within the TRM and proliferating cell clusters. This overlap suggested the two stimulation-induced clusters may have arisen from different transcriptional states. To test this hypothesis, we used the single-cell TCR sequencing data to trace clonal populations between unstimulated and stimulated datasets.

An evaluation of the top 50 clonotypes observed in the dataset revealed an overlap between the Stim-1 and the ISG and GZMK clusters (Figure 2D). In contrast, the $Stim_{EX}$ cluster shared many highly abundant clones with the T_{EX}-1 cluster, indicating clonal overlap between these populations. To explore this further, we next traced clones pre- or post-stimulation to investigate the clonal overlap with respect to stimulation and cluster identity. However, this analysis relied on the assumption that clones were sufficiently represented in both pre- and post-stimulation datasets. Indeed, it was observed that when clones are represented in 2 or more T-cells (clone size small), >60% of clones are captured within the stimulated dataset (i.e shared) (Figure 2E). Therefore, we proceeded with tracing the transcriptional responses of shared T-cell clones by linking their cluster identity pre- and post-stimulation. We observed that cells from the

Stim-1 cluster largely overlapped with unstimulated ISG and GZMK clusters (Figure 2F). Tracing unstimulated ISG clones, we observed clonal overlap that suggested stimulated ISG cells, either maintain their identity or adopt a GZMK or Stim-1 transcriptional phenotype. Similarly, unstimulated GZMK cells either retained GZMK identity or adopted ISG or Stim-1 transcriptional profiles post-stimulation. In contrast, clones from the $Stim_{EX}$ cluster were predominantly found to overlap with unstimulated T_{EX}-1 cluster with a minimal contribution from other unstimulated clusters (Figure 2G). As predicted, unstimulated T_{EX}-1 cluster clones overlapped with stimulated $Stim_{EX}$ or T_{EX}-1 clusters. Interestingly, this analysis also revealed that TCR-stimulation was capable of inducing a gene signature associated with T-cell activation in a subset of transcriptionally terminally exhausted T-cells (TCF7-TOX+PD1+) (Figure 1E & Figure 2B, C)

ISG cells largely retain their transcriptional identity upon TCR stimulation

To further understand the responsiveness to TCR stimulation across the dominant effector-like clusters, we isolated and projected them onto their own UMAP coordinates (Figure 3A). Subsequently, clones shared across pre- and post-stimulation datasets but whose cells were entirely contained within the ISG or GZMK clusters within the unstimulated dataset were identified (Figure 3B). This resulted in 26 and 53 unique clonotypes within unstimulated ISG or unstimulated GZMK clusters, respectively. Following TCR-stimulation, the majority of ISG T-cells retained their transcriptional identity (Figure 3C). In contrast, over 50% of unstimulated GZMK T-cells adopted a Stim-1 transcriptional identity following stimulation (Figure 3D), while the remaining proportion retained their GZMK identity. Interestingly, there was minimal adoption of an ISG signature following stimulation of GZMK clones. These data were further supported by pseudotime trajectory inference analysis, which revealed a trajectory of differentiation originating within the ISG cluster and transiting via GZMK population through to the Stim-1 cluster (Figure 3E). This trajectory was revealed using both a tree-based method (Slingshot) and a linear inference method (SCORPIUS; data not shown). Taken together, this data suggests a trajectory of ISG > GZMK > Stim-1, however, the transition from ISG > GZMK appears limiting as ISG cells were poorly responsive to TCR stimulation.

A type I interferon signature is associated with reduced transcriptional activity in ISG TILs

Given the diverse role of interferon signaling for the function of tumor-infiltrating T-cells, the relevance of ISG cells during tumor progression and immunotherapy remains elusive. We performed differential gene expression analysis and revealed a dominant signature enriched within the ISG population (Figure 4A). The top 10 differentially expressed genes identified within the ISG cluster were almost all found downstream of interferon signalling (Figure 4B). To understand the type of interferon signalling responsible, clusters were scored for genes contributing to a type I or type II interferon response (Figure 4C). Results showed the ISG cluster had enrichment for a type I, but not a type II interferon gene signature. Gene Ontology (GO) analysis was performed on the differentially up- or down-regulated genes within the ISG cluster relative to other clusters to unravel dominant biological processes associated with ISG cells. This analysis revealed a broad increase in translation related terms and type I IFN signalling responses (Figure 4D). Interestingly, down-regulated genes were enriched for GO terms associated with transcriptional regulation. This finding could explain our previous observation, that ISG cells poorly adopt new transcriptional states following TCR stimulation.

ISG cells are enriched in CD8+ TILs across various tumor types

To establish whether ISG cells could be identified in other microenvironments, we generated a specific gene signature using the top 10 differentially expressed genes from ISG cells within our data set (Figure 4B). We next examined if this signature could identify ISG cells in a publicly available HNSCC dataset in which an ISG cluster had previously been reported (Cillo et al. 2020). Indeed, using our curated ISG-signature, we were able to correctly identify a cluster of cells enriched for type I interferon genes (Supplementary Figure 2A).

To better understand the abundance of ISG cells within CD8+ T-cells in healthy and malignant tissues, we scored cells from a pan-cancer dataset for our ISG signature (Nicholas Borcherding 2022). Indeed, we could identify a fraction of T-cells highly enriched for our ISG-signature (Figure 5A). Next, we assessed the frequencies of ISG cells across normal and tumor tissues. Here, we found ISG cells to be significantly increased in tumor tissues, relative to normal tissue (Figure 5B). ISG cells were most frequent in Ovarian and Esophageal tumor types but also

detected to various degrees among all other tumor types assessed (Figure 5C). As expected ISG cells were solely enriched for type I but not type II IFN genes (Supplementary Figure 2B). We also assessed a COVID-19 dataset including some Influenza samples to determine if ISG cells are also enriched in the blood of virally infected patients (D. Wang et al. 2022). Indeed, in both conditions we observed a population of CD8+ T-cells enriched for our ISG signature (Supplementary Figure 2C) with a higher frequency in disease compared to healthy control samples (Supplementary Figure 2D), suggesting that the ISG cluster phenotype is not restricted to tumor immunity.

Finally, to better understand the functional role of ISG cells within the TME, we employed cell-cell communication analysis. Utilising a published HNSCC dataset containing an array of immune cell subsets (Cillo et al. 2020), we revealed that ISG cells served as the source for interactions with CD16 positive cells, as well as with NK cells and plasmacytoid dendritic cells (PDCs) (Figure 5D). ISG cells were also found to be a target for DC, B cell, and CD14 cell interactions. Hence, this data suggests ISG cells interact with key innate immune cell subsets within the TME and thus potentially are important orchestrator of anti-tumor immunity.

Discussion

HNSCC is a prevalent and complex disease with numerous etiological influences. For example, viral co-infection with HPV in Oropharyngeal HNSCC is associated with a better prognosis especially in early stage disease. As such, HPV- HNSCC presents as a more therapeutically challenging entity. Therefore, we sought to expand the knowledge base of CD8+ TIL landscape, specifically in treatment-naïve HPV- HNSCC patients. We employed a multimodal sequencing approach, together with an *ex vivo* TCR-stimulation, to facilitate tracing of transcriptional profiles and response capacity in CD8+ T-cell subsets.

Single-cell RNAseq of immune cell subsets has enabled in-depth mapping of the cellular heterogeneity of various disease conditions. However, traditionally this methodology only assesses the transcriptional state of cells *ex vivo*. Thus, capturing a snapshot of cellular transcriptomic landscape. Although, by leveraging an *ex vivo* perturbation coupled to sequencing

283 approaches, others have ascertained both *ex vivo* profiles and their subsequent activation
284 potentials. For example, a study by Szabo et al., 2019 performed *ex vivo* TCR-stimulation on T-
285 cells isolated from several healthy donor tissues. The authors were able to define both conserved
286 tissue signatures as well as the activation states of T-cells (Szabo et al. 2019). Using a similar
287 approach, we included TCR sequencing to facilitate tracing of transcriptional responses within
288 clonal populations of tumor-infiltrating T-cells. Notably, we observed two unique T-cell clusters
289 specifically induced by TCR-stimulation. Transcriptional signatures and clonal overlap suggest
290 these populations arose via stimulation of distinct *ex vivo* subsets. Importantly, we observed cells
291 that displayed a transcriptional program of terminal exhaustion (*TCF7-TOX+PDCD1+TIM3+*),
292 which retained substantial capacity to respond to TCR stimulation (Blank et al. 2019). These data
293 posit transcriptionally exhausted cells may retain substantive capacity to respond to stimulation.
294 Indeed, numerous scRNAseq studies have identified clusters of exhausted cells that
295 simultaneously express high levels of effector molecules (Andreatta et al. 2021; Quah et al.
296 2023). These observations highlight the need for multimodal data approaches to identify
297 prototypic exhausted T-cells while urging caution against defining exhaustion solely based on
298 transcriptional profiles.

299 IFN-I signaling in CD8+ T-cells is associated with both anti- and pro-tumoral function
300 (Zhou et al. 2020). Therefore, the clinical implications of an ISG-rich population is poorly
301 understood. Substantial challenges impede the experimental investigation of these cells and as
302 such our multi-modal sequencing approach has provided a comprehensive investigation of this
303 population. Our analysis has revealed that CD8+ ISG cells are a common feature of solid
304 malignancies and are specifically enriched within tumor tissue. Furthermore, we have found that
305 ISG cells are clonally related to GZMK-expressing CD8+ TILs. Pseudotime trajectory inference
306 suggested a differentiation pathway of ISG > GZMK > Stim-1 cells. However, experimental
307 perturbation revealed that ISG cells are transcriptionally stable and inert to TCR-stimulation. As
308 such, ISG cells may represent a barrier to the differentiation of GZMK cells and subsequent
309 terminally differentiated subsets. Although, numerous unknowns remain and ultimately further
310 experimentation is required to understand the functional implications of this differentiation
311 pathway and these cellular states.

This is not the first report to describe a population of cells enriched with interferon-stimulated genes. Indeed, numerous others have observed similar populations amongst malignant, infectious, and healthy tissues (X. Wang et al. 2022; Quah et al. 2023; Gideon et al. 2022; Cillo et al. 2020). However, the absence of specific cell-surface markers has hindered investigation efforts. Thus far, reports of this population have been limited to mere observation of their appearance. Illustrative of this, Wang and colleagues identified a subset of ISG cells within sequencing data of healthy PBMCs. Despite their efforts, the authors were unable to experimentally isolate this population and thus were limited in the functional analysis that could be performed (X. Wang et al. 2022). Therefore, alternative markers and/or strategies to identify and isolate cells with this cellular state are required. In absence of this, our multimodal sequencing and experimental perturbation approach has provided novel insights into ISG CD8+ TILs.

Ex vivo stimulation additionally revealed a cluster of cells that predominantly arose from ISG and GZMK clusters. These clusters had substantial clonal overlap and trajectory inference suggested ISG cells transition through a GZMK phenotype towards the fully activated T-cell state. However, further interrogation of the clonal response to stimulation revealed that ISG cells are transcriptionally inert to TCR-stimulation. The relationship between GZMK and ISG cells is notable as others have demonstrated GZMK expression within solid tumors is associated with improved patient outcomes (Rooney et al. 2015; C. Zheng et al. 2017). Although, the nature of this association is unclear, as GZMK is usually correlated with innate cells and naïve phenotypes. For example, GZMK is more dominantly expressed within immature NK cells. However, GZMK expression within CD8+ T-cells is predominantly observed within central memory and effector memory subsets (Duquette et al. 2023). Thus, supporting the notion that GZMK expression within CD8+ T-cells may correlate with favourable prognosis. Although, it has been observed that GZMK+ CD8+ T-cells are poorly cytotoxic and instead produce IFNγ (Harari et al. 2009; Duquette et al. 2023). Interestingly, others have differential effects of TCR or cytokine stimulation on GZMK expression. Namely, that TCR-stimulation induces the release of GZMK and increase in GZMB expression. Conversely, cytokine-based stimulation drives accumulation of GZMK (Duquette et al. 2023). These findings are consistent with our results which demonstrated TCR-based stimulation drives GZMK cells to down-regulate GZMK and up-regulate GZMB as they differentiate towards a more terminal effector phenotype. Therefore,

these data suggest GZMK positivity marks CD8+ T-cells which are not yet terminally differentiated and instead possess a more memory-like phenotype. Additionally, our data suggests ISG cells differentiate into GZMK cells however, they possess relative transcriptional stability. As such, TCR-stimulation is insufficient to drive ISG cells to adopt a GZMK transcriptional phenotype. Thus, ISG cells could function as a barrier within this differentiation trajectory. The functional consequences of this are unknown. Given the above model, accumulation of ISG cells could prevent the development of more terminally differentiated anti-tumoral responses via GZMK intermediaries. However, GZMK+ CD8+ T-cells have been observed within tumor stroma and have been implicated in poor prognosis (Tiberti et al. 2022). Additionally, GZMK CD8+ TILs have been described as a transition state on the trajectory towards exhaustion (C. Zheng et al. 2017; Sun et al. 2022). This is consistent with reports showing IFN-I signalling as a driver of T-cell exhaustion (Chen et al. 2022; Sumida et al. 2022). Therefore, the functional consequences of ISG and GZMK TILs is poorly defined. Further studies are required to better understand the dynamics and function of T cell clusters infiltrating tumor tissues.

Methods

Patient Samples

A total of eight patients who had provided informed consent, were included in this study. Samples were obtained from surgical resections of primary HNSCC tumors. All patients presented with oral cavity squamous cell carcinoma and were confirmed to be human papillomavirus (HPV) negative. Fresh HNSCC tumors were collected at the time of resection of the primary tumor and sampled by a pathologist prior to fixation. Fresh tissue was processed to isolate tumor cells and immune cells prior to preservation and storage in liquid nitrogen. The patients enrolled in this study were treatment naïve and characteristics can be found in Figure 1A. Ethical approval for this study was obtained from the Royal Brisbane and Women's Hospital Human Research Ethics Committee and the QIMR Berghofer Human Research Ethics Committee, HREC/18/QRBW/245.

Single-cell RNA sequencing

Cells from each patient were cultured as single-cell suspensions and were either stimulated using CD3/CD28 beads or left unstimulated for a duration of 5 hours. Following culture, the cells were sorted using fluorescence-activated cell sorting to isolate live CD45+CD3+CD4-CD8+ cells. Patient samples were sequenced as two unstimulated and two stimulated samples where each sequencing sample represented a pool of 4 patients. As such, approximately 10,000 cells per sample pool were carried forward into the 10x Genomics Single-cell 5' library pipeline. The libraries were sequenced using a NextSeq 550 (Illumina). The sequencing was performed at QIMR Berghofer Medical Institute.

scRNAseq pre-processing

Sequencing reads were processed using cellranger (version 3.1.0) and reads were aligned to human reference genome GRCH38-3.0.0. Output from cellranger was processed using Seurat (version 4.3.0). Each sequencing sample was filtered to keep only cells that had a minimum of 200 features and keep features that were detected in a minimum of 3 cells. Subsequently, the two unstimulated samples were merged and the two stimulated samples were merged to give two Seurat objects. These Seurat objects were further filtered to remove cells with greater than 2,500 features or greater than 10% mitochondrial content. Filtering resulted in 5,785 cells with 15,429 features in the unstimulated dataset and 6,042 cells with 15,618 features in the stimulated dataset. Datasets were normalised using LogNormalisation with a scale factor of 10,000. Subsequently, mitochondrial percentage and nCount variables were regressed out using a linear model. Unstimulated and Stimulated datasets were integrated using the Seurat integration pipeline. Unless otherwise stated integration functions/pipeline was executed using default function variables. Integration anchors were calculated using "cca" reduction, "LogNormalize" as a normalization method, and "rann" as the Nearest Neighbour method. Integration resulted in a dataset of 18,295 features across 11,827 cells.

scRNAseq analysis

Dimension reduction and cluster identification: The top 30 PCAs were calculated on the integrated dataset and Nearest-neighbors computed using the top 20 dimensions. Clusters were determined using a cluster resolution of "0.4". UMAP in figure 1 was generated using top 20

PCA dimensions, the "uwot" algorithm, n.neighbors = 30, and min.dist = 0.3. Following UMAP dimension reduction calculation, clusters were investigated both with manually curated gene signatures and with the use of SingleR (version 2.0.0) to classify cells using data from celldex (version 1.8.0). Two low abundance clusters were removed that were identified as either having high mitochondrial content or a myeloid signature. UMAP projection was recalculated following the removal of these clusters, using the same parameters as previously stated. Therefore, after cluster identification the dataset contained 20,295 features across 11,658 cells with 5,724 cells from the unstimulated treatment condition and 5,934 cells from the stimulated treatment condition. Subsequently, unconventional T-cell clusters were subsetted from the dataset resulting in unconventional T-cell-only and CD8-only datasets. UMAP projections were recalculated for these datasets using the top 20 PCA dimensions, n.neighbors = 50, and a min.dist of 0.1 for CD8-only dataset or 0.5 for the unconventional T-cell-only dataset. The unconventional T-cell-only dataset consisted of 20,295 features across 970 cells. The CD8-only dataset consisted of 20,295 features across 10,688 cells, 5,165 of which originated from the unstimulated treatment condition and 5,523 from the stimulated treatment condition.

Differential gene expression: Calculations to determine differentially expressed genes between clusters or conditions was performed using wilcox test implemented via the standard Seurat analysis pipeline. Analysis was performed using the RNA data slot of the Seurat object.

Differentially expressed transcription factors: To determine the differential expression of transcription factors, the list of differentially expressed genes was cross-referenced with a curated database of RNA polymerase II regulated transcription factors (TFcheckpoint; http://www.tfcheckpoint.org).

Gene ontology analysis: Briefly, differentially expressed genes for the ISG cluster were identified using Seurat's FindMarkers() function. Genes identified as significantly (adjusted p.value < 0.5) up- or down-regulated were then passed to the enrichR package (version 3.1) to identify enriched terms using the GO_Biological_Process_2021 database. The top 10 enriched terms were then visualised using SCpubr (version 1.1.1).

Signature scoring: Signature score calculated using UCell (version 2.2.0) with signatures for type I and II IFN obtained from (Azizi et al. 2018).

Cell-cell communication analysis: Cell-cell communication was performed using the R package "liana" (version 0.1.12). In brief, cell-cell communication networks were calculated using the following methods "natmi", "connectome", "logfc", "sca", and "cellphonedb". The scores from these methods were subsequently aggregated and only interactions concordant between methods were kept. This analysis followed the recommended analytical pipeline for the "liana" package.

Trajectory Inference: Trajectory inference was performed using the dynverse (Cannoodt and Saelens 2023) collection of packages. Analysis was performed using standard pipeline with default parameters and without supplying any priors for both slingshot and Scorpius trajectory inference algorithms.

scRNAseq visualisation

Imputation: Imputation of gene expression was performed and used in certain visualisations where indicated. Imputed values were not used for any downstream analysis and were exclusively used in indicated visualisations. Imputation was performed using the "RunALRA" function in Seurat and increased the percentage of non-zero values in the dataset from 29.63% to 38.95%.

Density based UMAP visualisation: The Nebulosa package (version 1.8.0) together with scCustomize package (version 1.1.1) were used to visualise gene expression on UMAP projections and expression density.

Color scheme: Where possible the uniform, colorblind-friendly batlow (Crameri, Shephard, and Heron 2020) color pallet was used for data visualisation. The color palette was accessed using the scico package (version 1.3.1).

Single-cell TCR sequencing analysis

Pre-processing: Single-cell TCR sequencing data were aligned using cellranger pipeline (version 3.1.0) to the human VDJ reference (vdj_GRCh38_alts_ensembl-3.1.0-3.1.0). TCR data was subsequently processed using scRepertoire (version 1.8.0). TCR data was filtered such that if cells had multiple alpha or beta chains identified, only the top expressing chain was retained.

Additionally, unless otherwise stated, clone identity was defined by the CDR3 amino acid sequence.

Clone size definitions: Abundance of clones was calculated per stimulation condition and binned according to the following definitions. Single (x = 1), small (1 < x < =5), medium (5 < x <=10), large (10 < x <=20) and hyperexpanded (20 < x <= 150). Where x = number of cells with exact CDR3 amino acid sequence. Size cut-offs were determined empirically using summary statistics of clone abundances across the dataset.

External datasets

uTILity: The pan-cancer "uTILity" dataset was acquired from (Nicholas Borcherding 2022) circa 13.10.2022. The dataset was filtered to retain only cells identified as CD8 T-cells and only Tumor and Normal tissue types were retained. Subsetted dataset was normalized and reintegrated using the harmony package (version 0.1.1) to remove "Cohort" effect. UMAP coordinates and clusters were recalculated following harmonization, using the standard Seurat analysis pipeline.

HNSCC: For validation of ISG gene signature and cell-cell communication analysis, the HNSCC TILs dataset published in (Cillo et al. 2020) was used. Processed data was downloaded from (GSE139324)[https://www.ncbi.nlm.nih.gov/geo/query/acc.cgi?acc=GSE139324]. Metadata for this dataset was obtained through contact with the lead author/s.

COMBAT dataset: The Covid-19 and Infleunza scRNAseq dataset was downloaded from https://zenodo.org/records/6120249 (COvid-19 Multi-omics Blood ATlas (COMBAT) Consortium 2022)

Figure preparation

Figures were arranged and formatted using Adobe Illustrator (version 27.5) and/or GraphPad Prism (version 9).

Table 1: Analysis packages used

Package/environment	Version	Reference
celldex	1.8.0	(Aran et al. 2019)
cellranger	3.1.0	(G. X. Y. Zheng et al. 2017)
Dynverse	0.1.2	(Cannoodt and Saelens 2023)
enrichR	3.1	(Jawaid 2023)
harmony	0.1.1	(Korsunsky et al. 2023)
liana	0.1.12	(Dimitrov et al. 2022)
Nebulosa	1.8.0	(Alquicira-Hernandez and Powell 2021)
R	4.1.1	(R Core Team 2023)
RStudio	2023.03.0 +386	(RStudio Team 2020)
scCustomize	1.1.1	(Marsh 2023)
scico	1.3.1	(Pedersen and Crameri 2023)

SCpubr	1.1.1	(Blanco-Carmona 2022)
scRepertoire	1.8.0	(Nick Borcherding 2022)
Seurat	4.3.0	(Hao et al. 2021)
SeuratDisk	0.0.0.9020	(Hoffman, Paul 2023)
SeuratObject	4.1.3	(Satija, Hoffman, et al. 2023)
SeuratWrappers	0.3.1	(Satija, Butler, et al. 2023)
SingleR	2.0.0	(Aran et al. 2019)
System	x86_64, darwin17.0	
UCell	2.2.0	(Andreatta and Carmona 2021)

481 Table depicting the analysis packages and the software environments used within this manuscript

482 **Availability of data and materials**

483 The single-cell RNA/TCR sequencing dataset generated will be made available upon reasonable
484 request and approval of HREC. All code used to generate figures can be found under the relevant
485 repository at https://github.com/BaldLab. All other data generated are available upon request.

Competing interests

N.B. is a current employee of Omniscope, Inc and has consulted for Starling Biosciences and Santa Ana Bio in the last 36 months. All other authors declare that they have no competing interests.

Funding

T.B. is funded by the Deutsche Forschungsgemeinschaft (DFG, German Research Foundation) under Germany's Excellence Strategy – EXC2151–390873048 and the Melanoma Research Alliance (https://doi.org/10.48050/pc.gr.91568). K.T is funded by DFG Excellence Strategy EXC2151–390873048 and EXC2047-390873048.

Authors contributions

Conceptualization – D.C, M.B and T.B

Methodology – D.C, M.B,

Software – D.C, T.K, L.M.S, D.P, N.B

Formal Analysis – D.C, T.K, L.M.S, D.P, N.B

Investigation – D.C, N.S, M.B, T.B

Resources – N.B, M.H, T.B, K.T, S.P, Ma.Ba, J.M, B.H

Data curation – D.C, L.T.K, N.B

Writing (Original Draft) – D.C, M.B, T.B

Writing (Review & Editing) – all authors

Visualization – D.C, N.B

Supervision – D.C, M.B and T.B

Funding acquisition – T.B

Project administration – T.B

Acknowledgements

Firstly, we wish to extend our appreciation for the patients whom provided their samples, without which, this study would not have been possible. Additionally, we express our gratitude to the flow cytometry and next generation sequencing facilities of QIMR Berghofer Medical Research Institute. We thank aimed analytics GmbH for bioinformatics support. We thank Christian Engwerda from QIMR Berghofer Medical Research Institute for advice and support on this manuscript.

References

Alquicira-Hernandez, Jose, and Joseph E. Powell. 2021. "Nebulosa Recovers Single-Cell Gene Expression Signals by Kernel Density Estimation." *Bioinformatics (Oxford, England)* 37 (16): 2485–87. https://doi.org/10.1093/bioinformatics/btab003.

Andersen, Anne Skou, Anne Sophie Koldjær Sølling, Therese Ovesen, and Maria Rusan. 2014. "The Interplay between HPV and Host Immunity in Head and Neck Squamous Cell Carcinoma." *International Journal of Cancer* 134 (12): 2755–63. https://doi.org/10.1002/ijc.28411.

Andreatta, Massimo, and Santiago J. Carmona. 2021. "UCell: Robust and Scalable Single-Cell Gene Signature Scoring." *Computational and Structural Biotechnology Journal* 19: 3796–98. https://doi.org/10.1016/j.csbj.2021.06.043.

Andreatta, Massimo, Jesus Corria-Osorio, Sören Müller, Rafael Cubas, George Coukos, and Santiago J. Carmona. 2021. "Interpretation of T Cell States from Single-Cell Transcriptomics Data Using Reference Atlases." *Nature Communications* 12 (1): 2965. https://doi.org/10.1038/s41467-021-23324-4.

Ang, K. Kian, Jonathan Harris, Richard Wheeler, Randal Weber, David I. Rosenthal, Phuc Felix Nguyen-Tân, William H. Westra, et al. 2010. "Human Papillomavirus and Survival of Patients with Oropharyngeal Cancer." *The New England Journal of Medicine* 363 (1): 24–35. https://doi.org/10.1056/NEJMoa0912217.

Aran, Dvir, Agnieszka P. Looney, Leqian Liu, Esther Wu, Valerie Fong, Austin Hsu, Suzanna Chak, et al. 2019. "Reference-Based Analysis of Lung Single-Cell Sequencing Reveals a Transitional Profibrotic Macrophage." *Nature Immunology* 20 (2): 163–72. https://doi.org/10.1038/s41590-018-0276-y.

Azizi, Elham, Ambrose J. Carr, George Plitas, Andrew E. Cornish, Catherine Konopacki, Sandhya Prabhakaran, Juozas Nainys, et al. 2018. "Single-Cell Map of Diverse Immune Phenotypes in the Breast Tumor Microenvironment." *Cell* 174 (5): 1293-1308.e36. https://doi.org/10.1016/j.cell.2018.05.060.

Bald, Tobias, Jennifer Landsberg, Dorys Lopez-Ramos, Marcel Renn, Nicole Glodde, Philipp Jansen, Evelyn Gaffal, et al. 2014. “Immune Cell-Poor Melanomas Benefit from PD-1 Blockade after Targeted Type I IFN Activation.” *Cancer Discovery* 4 (6): 674–87. https://doi.org/10.1158/2159-8290.CD-13-0458.

Blanco-Carmona, Enrique. 2022. “Generating Publication Ready Visualizations for Single Cell Transcriptomics Using SCpubr.” bioRxiv. https://doi.org/10.1101/2022.02.28.482303.

Blank, Christian U., W. Nicholas Haining, Werner Held, Patrick G. Hogan, Axel Kallies, Enrico Lugli, Rachel C. Lynn, et al. 2019. “Defining ‘T Cell Exhaustion.’” *Nature Reviews. Immunology* 19 (11): 665–74. https://doi.org/10.1038/s41577-019-0221-9.

Borcherding, Nicholas. 2022. “Utility: Collection of Tumor-Infiltrating Lymphocyte Single-Cell Experiments with TCR.” Zenodo. https://doi.org/10.5281/zenodo.6325603.

Borcherding, Nick. 2022. “scRepertoire: A Toolkit for Single-Cell Immune Receptor Profiling.”

Burtness, Barbara, Kevin J Harrington, Richard Greil, Denis Soulières, Makoto Tahara, Gilberto de Castro, Amanda Psyrri, et al. 2019. “Pembrolizumab Alone or with Chemotherapy versus Cetuximab with Chemotherapy for Recurrent or Metastatic Squamous Cell Carcinoma of the Head and Neck (KEYNOTE-048): A Randomised, Open-Label, Phase 3 Study.” *The Lancet* 394 (10212): 1915–28. https://doi.org/10.1016/S0140-6736(19)32591-7.

Cannoodt, Robrecht, and Wouter Saelens. 2023. “Dyno: Set of Packages for Doing Trajectory Inference on Single-Cell Data.” https://github.com/dynverse/dyno.

Chen, Weixin, Jia Ming Nickolas Teo, Siu Wah Yau, Melody Yee-Man Wong, Chun-Nam Lok, Chi-Ming Che, Asif Javed, Yuanhua Huang, Stephanie Ma, and Guang Sheng Ling. 2022. “Chronic Type I Interferon Signaling Promotes Lipid-Peroxidation-Driven Terminal CD8+ T Cell Exhaustion and Curtails Anti-PD-1 Efficacy.” *Cell Reports* 41 (7): 111647. https://doi.org/10.1016/j.celrep.2022.111647.

Cillo, Anthony R., Cornelius H. L. Kürten, Tracy Tabib, Zengbiao Qi, Sayali Onkar, Ting Wang, Angen Liu, et al. 2020. “Immune Landscape of Viral- and Carcinogen-Driven Head and

Neck Cancer." *Immunity* 52 (1): 183-199.e9. https://doi.org/10.1016/j.immuni.2019.11.014.

COvid-19 Multi-omics Blood ATlas (COMBAT) Consortium. 2022. "A Blood Atlas of COVID-19 Defines Hallmarks of Disease Severity and Specificity." *Cell* 185 (5): 916-938.e58. https://doi.org/10.1016/j.cell.2022.01.012.

Crameri, Fabio, Grace E. Shephard, and Philip J. Heron. 2020. "The Misuse of Colour in Science Communication." *Nature Communications* 11 (1): 5444. https://doi.org/10.1038/s41467-020-19160-7.

Curtsinger, Julie M., and Matthew F. Mescher. 2010. "Inflammatory Cytokines as a Third Signal for T Cell Activation." *Current Opinion in Immunology* 22 (3): 333–40. https://doi.org/10.1016/j.coi.2010.02.013.

Diamond, Mark S., Michelle Kinder, Hirokazu Matsushita, Mona Mashayekhi, Gavin P. Dunn, Jessica M. Archambault, Hsiaoju Lee, et al. 2011. "Type I Interferon Is Selectively Required by Dendritic Cells for Immune Rejection of Tumors." *Journal of Experimental Medicine* 208 (10): 1989–2003. https://doi.org/10.1084/jem.20101158.

Dimitrov, Daniel, Dénes Türei, Martin Garrido-Rodriguez, Paul L. Burmedi, James S. Nagai, Charlotte Boys, Ricardo O. Ramirez Flores, et al. 2022. "Comparison of Methods and Resources for Cell-Cell Communication Inference from Single-Cell RNA-Seq Data." *Nature Communications* 13 (1): 3224. https://doi.org/10.1038/s41467-022-30755-0.

Duquette, Danielle, Cathal Harmon, Alexandra Zaborowski, Xavier Michelet, Cliona O'Farrelly, Des Winter, Hui-Fern Koay, and Lydia Lynch. 2023. "Human Granzyme K Is a Feature of Innate T Cells in Blood, Tissues, and Tumors, Responding to Cytokines Rather than TCR Stimulation." *The Journal of Immunology* 211 (4): 633–47. https://doi.org/10.4049/jimmunol.2300083.

Ferris, R.L., G. Blumenschein, J. Fayette, J. Guigay, A.D. Colevas, L. Licitra, K. Harrington, et al. 2016. "Nivolumab for Recurrent Squamous-Cell Carcinoma of the Head and Neck."

The New England Journal of Medicine 375 (19): 1856–67. https://doi.org/10.1056/NEJMoa1602252.

Fuertes, Mercedes B., Aalok K. Kacha, Justin Kline, Seng-Ryong Woo, David M. Kranz, Kenneth M. Murphy, and Thomas F. Gajewski. 2011. "Host Type I IFN Signals Are Required for Antitumor CD8+ T Cell Responses through CD8α+ Dendritic Cells." *Journal of Experimental Medicine* 208 (10): 2005–16. https://doi.org/10.1084/jem.20101159.

Fung, Nicholas, Farhoud Faraji, Hyunseok Kang, and Carole Fakhry. 2017. "The Role of Human Papillomavirus on the Prognosis and Treatment of Oropharyngeal Carcinoma." *Cancer Metastasis Reviews* 36 (3): 449–61. https://doi.org/10.1007/s10555-017-9686-9.

Gherardin, Nicholas A, Michael NT Souter, Hui-Fern Koay, Kirstie M Mangas, Torsten Seemann, Timothy P Stinear, Sidonia BG Eckle, et al. 2018. "Human Blood MAIT Cell Subsets Defined Using MR1 Tetramers." *Immunology and Cell Biology* 96 (5): 507–25. https://doi.org/10.1111/imcb.12021.

Gideon, Hannah P., Travis K. Hughes, Constantine N. Tzouanas, Marc H. Wadsworth, Ang Andy Tu, Todd M. Gierahn, Joshua M. Peters, et al. 2022. "Multimodal Profiling of Lung Granulomas in Macaques Reveals Cellular Correlates of Tuberculosis Control." *Immunity* 55 (5): 827-846.e10. https://doi.org/10.1016/j.immuni.2022.04.004.

Hao, Yuhan, Stephanie Hao, Erica Andersen-Nissen, William M. Mauck, Shiwei Zheng, Andrew Butler, Maddie J. Lee, et al. 2021. "Integrated Analysis of Multimodal Single-Cell Data." *Cell* 184 (13): 3573-3587.e29. https://doi.org/10.1016/j.cell.2021.04.048.

Harari, Alexandre, Felicitas Bellutti Enders, Cristina Cellerai, Pierre-Alexandre Bart, and Giuseppe Pantaleo. 2009. "Distinct Profiles of Cytotoxic Granules in Memory CD8 T Cells Correlate with Function, Differentiation Stage, and Antigen Exposure." *Journal of Virology* 83 (7): 2862–71. https://doi.org/10.1128/JVI.02528-08.

Hoffman, Paul. 2023. "Interfaces for HDF5-Based Single Cell File Formats." https://mojaveazure.github.io/seurat-disk/.

624 Jawaid, Wajid. 2023. “enrichR: Provides an R Interface to ‘Enrichr.’” https://CRAN.R-
625 project.org/package=enrichR.

626 Johnson, Daniel E., Barbara Burtness, C. René Leemans, Vivian Wai Yan Lui, Julie E. Bauman,
627 and Jennifer R. Grandis. 2020. “Head and Neck Squamous Cell Carcinoma.” *Nature*
628 *Reviews. Disease Primers* 6 (1): 92. https://doi.org/10.1038/s41572-020-00224-3.

629 Kalyan, Shirin, and Dieter Kabelitz. 2013. “Defining the Nature of Human Γδ T Cells: A
630 Biographical Sketch of the Highly Empathetic.” *Cellular and Molecular Immunology* 10
631 (1): 21–29. https://doi.org/10.1038/cmi.2012.44.

632 Korsunsky, Ilya, Martin Hemberg, Nikolaos Patikas, Hongcheng Yao, Nghia Millard, Jean Fan,
633 Kamil Slowikowski, and Soumya Raychaudhuri. 2023. “Harmony: Fast, Sensitive, and
634 Accurate Integration of Single Cell Data.” https://CRAN.R-
635 project.org/package=harmony.

636 Lassen, Pernille, Jesper G. Eriksen, Stephen Hamilton-Dutoit, Trine Tramm, Jan Alsner, and
637 Jens Overgaard. 2009. “Effect of HPV-Associated p16INK4A Expression on Response to
638 Radiotherapy and Survival in Squamous Cell Carcinoma of the Head and Neck.” *Journal*
639 *of Clinical Oncology: Official Journal of the American Society of Clinical Oncology* 27
640 (12): 1992–98. https://doi.org/10.1200/JCO.2008.20.2853.

641 Marsh, Samuel. 2023. “scCustomize: Custom Visualizations & Functions for Streamlined
642 Analyses of Single Cell Sequencing.” https://CRAN.R-project.org/package=scCustomize.

643 Ndiaye, Cathy, Marisa Mena, Laia Alemany, Marc Arbyn, Xavier Castellsagué, Louise Laporte,
644 F. Xavier Bosch, Silvia de Sanjosé, and Helen Trottier. 2014. “HPV DNA, E6/E7
645 mRNA, and p16INK4a Detection in Head and Neck Cancers: A Systematic Review and
646 Meta-Analysis.” *The Lancet. Oncology* 15 (12): 1319–31. https://doi.org/10.1016/S1470-
647 2045(14)70471-1.

648 Nelson, Heather H., Michael Pawlita, Dominique S. Michaud, Michael McClean, Scott M.
649 Langevin, Melissa N. Eliot, and Karl T. Kelsey. 2017. “Immune Response to HPV16 E6

and E7 Proteins and Patient Outcomes in Head and Neck Cancer." *JAMA Oncology* 3 (2): 178–85. https://doi.org/10.1001/jamaoncol.2016.4500.

Pedersen, Thomas Lin, and Fabio Crameri. 2023. "Scico: Colour Palettes Based on the Scientific Colour-Maps." https://CRAN.R-project.org/package=scico.

Quah, Hong Sheng, Elaine Yiqun Cao, Lisda Suteja, Constance H. Li, Hui Sun Leong, Fui Teen Chong, Shilpi Gupta, et al. 2023. "Single Cell Analysis in Head and Neck Cancer Reveals Potential Immune Evasion Mechanisms during Early Metastasis." *Nature Communications* 14 (1): 1680. https://doi.org/10.1038/s41467-023-37379-y.

R Core Team. 2023. "R: A Language and Environment for Statistical Computing." Vienna, Austria: R Foundation for Statistical Computing. https://www.R-project.org/.

Rooney, Michael S., Sachet A. Shukla, Catherine J. Wu, Gad Getz, and Nir Hacohen. 2015. "Molecular and Genetic Properties of Tumors Associated with Local Immune Cytolytic Activity." *Cell* 160 (1–2): 48–61. https://doi.org/10.1016/j.cell.2014.12.033.

RStudio Team. 2020. "RStudio: Integrated Development Environment for R." Boston, MA: RStudio, PBC. http://www.rstudio.com/.

Ruotsalainen, Janne, Dorys Lopez-Ramos, Meri Rogava, Naveen Shridhar, Nicole Glodde, Evelyn Gaffal, Michael Hölzel, Tobias Bald, and Thomas Tüting. 2021. "The Myeloid Cell Type I IFN System Promotes Antitumor Immunity over Pro-Tumoral Inflammation in Cancer T-Cell Therapy." *Clinical & Translational Immunology* 10 (4): e1276. https://doi.org/10.1002/cti2.1276.

Sacco, Assuntina G., Ruifeng Chen, Francis P. Worden, Deborah J. L. Wong, Douglas Adkins, Paul Swiecicki, Wanxing Chai-Ho, et al. 2021. "Pembrolizumab plus Cetuximab in Patients with Recurrent or Metastatic Head and Neck Squamous Cell Carcinoma: An Open-Label, Multi-Arm, Non-Randomised, Multicentre, Phase 2 Trial." *The Lancet. Oncology* 22 (6): 883–92. https://doi.org/10.1016/S1470-2045(21)00136-4.

Sade-Feldman, Moshe, Keren Yizhak, Stacey L. Bjorgaard, John P. Ray, Carl G. de Boer, Russell W. Jenkins, David J. Lieb, et al. 2018. "Defining T Cell States Associated with

677 Response to Checkpoint Immunotherapy in Melanoma." *Cell* 175 (4): 998-1013.e20.
678 https://doi.org/10.1016/j.cell.2018.10.038.

679 Satija, Rahul, Andrew Butler, Paul Hoffman, and Tim Stuart. 2023. "SeuratWrappers:
680 Community-Provided Methods and Extensions for the Seurat Object."

681 Satija, Rahul, Paul Hoffman, Yuhan Hao, Austin Hartman, Gesmira Molla, Andrew Butler, and
682 Tim Stuart. 2023. "SeuratObject: Data Structures for Single Cell Data." https://CRAN.R-
683 project.org/package=SeuratObject.

684 Sumida, Tomokazu S., Shai Dulberg, Jonas C. Schupp, Matthew R. Lincoln, Helen A. Stillwell,
685 Pierre-Paul Axisa, Michela Comi, et al. 2022. "Type I Interferon Transcriptional Network
686 Regulates Expression of Coinhibitory Receptors in Human T Cells." *Nature Immunology*
687 23 (4): 632–42. https://doi.org/10.1038/s41590-022-01152-y.

688 Sun, Keyong, Runda Xu, Fuhai Ma, Naixue Yang, Yang Li, Xiaofeng Sun, Peng Jin, et al. 2022.
689 "scRNA-Seq of Gastric Tumor Shows Complex Intercellular Interaction with an
690 Alternative T Cell Exhaustion Trajectory." *Nature Communications* 13 (August): 4943.
691 https://doi.org/10.1038/s41467-022-32627-z.

692 Szabo, Peter A., Hanna Mendes Levitin, Michelle Miron, Mark E. Snyder, Takashi Senda,
693 Jinzhou Yuan, Yim Ling Cheng, et al. 2019. "Single-Cell Transcriptomics of Human T
694 Cells Reveals Tissue and Activation Signatures in Health and Disease." *Nature*
695 *Communications* 10 (1): 4706. https://doi.org/10.1038/s41467-019-12464-3.

696 Tiberti, Silvia, Carlotta Catozzi, Ottavio Croci, Mattia Ballerini, Danilo Cagnina, Chiara Soriani,
697 Caterina Scirgolea, et al. 2022. "GZMKhigh CD8+ T Effector Memory Cells Are
698 Associated with CD15high Neutrophil Abundance in Non-Metastatic Colorectal Tumors
699 and Predict Poor Clinical Outcome." *Nature Communications* 13 (1): 6752.
700 https://doi.org/10.1038/s41467-022-34467-3.

701 Vos, Joris L., Joris B. W. Elbers, Oscar Krijgsman, Joleen J. H. Traets, Xiaohang Qiao, Anne M.
702 van der Leun, Yoni Lubeck, et al. 2021. "Neoadjuvant Immunotherapy with Nivolumab
703 and Ipilimumab Induces Major Pathological Responses in Patients with Head and Neck

Squamous Cell Carcinoma." *Nature Communications* 12 (1): 7348. https://doi.org/10.1038/s41467-021-26472-9.

Wang, Dapeng, Vinod Kumar, Katie L Burnham, Alexander J Mentzer, Brian D Marsden, and Julian C Knight. 2022. "COMBATdb: A Database for the COVID-19 Multi-Omics Blood ATlas." *Nucleic Acids Research* 51 (D1): D896–905. https://doi.org/10.1093/nar/gkac1019.

Wang, Xuefei, Xiangru Shen, Shan Chen, Hongyi Liu, Ni Hong, Hanbing Zhong, Xi Chen, and Wenfei Jin. 2022. "Reinvestigation of Classic T Cell Subsets and Identification of Novel Cell Subpopulations by Single-Cell RNA Sequencing." *Journal of Immunology (Baltimore, Md.: 1950)* 208 (2): 396–406. https://doi.org/10.4049/jimmunol.2100581.

Yu, Renren, Bo Zhu, and Degao Chen. 2022. "Type I Interferon-Mediated Tumor Immunity and Its Role in Immunotherapy." *Cellular and Molecular Life Sciences* 79 (3): 191. https://doi.org/10.1007/s00018-022-04219-z.

Zheng, Chunhong, Liangtao Zheng, Jae-Kwang Yoo, Huahu Guo, Yuanyuan Zhang, Xinyi Guo, Boxi Kang, et al. 2017. "Landscape of Infiltrating T Cells in Liver Cancer Revealed by Single-Cell Sequencing." *Cell* 169 (7): 1342-1356.e16. https://doi.org/10.1016/j.cell.2017.05.035.

Zheng, Grace X. Y., Jessica M. Terry, Phillip Belgrader, Paul Ryvkin, Zachary W. Bent, Ryan Wilson, Solongo B. Ziraldo, et al. 2017. "Massively Parallel Digital Transcriptional Profiling of Single Cells." *Nature Communications* 8 (1): 14049. https://doi.org/10.1038/ncomms14049.

Zhou, Lili, Yuqi Zhang, Yongqiang Wang, Meirong Zhang, Wenhuan Sun, Tong Dai, Aijun Wang, et al. 2020. "A Dual Role of Type I Interferons in Antitumor Immunity." *Advanced Biosystems* 4 (11): e1900237. https://doi.org/10.1002/adbi.201900237.

Figure Legends

Figure 1: The transcriptional landscape of tumor-infiltrating CD8+ TILs in treatment-naive in head and neck squamous cell carcinoma (HNSCC) patients

(A) schematic detailing experimental setup used to generate the dataset. In brief, the tumors from eight head and neck squamous cell carcinoma (HNSCC) patients were digested and processed into a single-cell suspension. The cell suspension was cultured for 5 hours with or without CD3/CD28 T-cell stimulation. Subsequently, the cells were sorted for CD3+CD4-CD8+ T-cells and subjected to 10X single-cell sequencing. Key patient characteristics are listed in the table below the schematic. All patients were HPV negative, treatment naïve, and samples were from primary tumors. Schematic created with BioRender.com (B) UMAP projection of all cells that passed QC inclusion criteria. (C–G) UMAP projections highlighting (first column) clusters identified and subsequently the expression density of key genes used in their identification. (G) MAIT-cell identity is highlighted using the joint density expression of TRAV1-2 and KLRB1 (H) Barplot showing the frequency of each cluster identified as a proportion of the entire dataset.

Supplementary Figure 1: Transcriptional profile of CD8+ T-cell and unconventional T-cell subsets in head and neck squamous cell carcinoma

(A) Stacked barplot showing the relative proportion of each cluster by stimulation status. (B) Stacked violin plots of key genes across identified clusters. (C) UMAP projection of unconventional T-cells identified within sequencing dataset. (D) Heatmap of unconventional T-cell clusters showing gamma-delta TCR genes detected and key markers of MAIT-cells. (E) Stacked violin plots of key T-cell receptor genes. (F) Heatmap of top differentially expressed genes (log2FC > 1) with selected genes annotated. (G) Heatmap of the average expression of differentially expressed transcription factors.

Figure 2: *Ex vivo* TCR stimulation induced transcriptional states develop from distinct unstimulated origins

(A) UMAP projection of CD8+ TILs identified in HNSCC patients after removal of unconventional T-cell subsets. (B) Heatmap of DEGs found to be upregulated (> 0.5 log2FC) in both stimulated-1 and stim-exhausted clusters, selected genes are annotated. (C) Heatmap of genes found to be significantly differentially expressed (>0.5 log2FC) between stim-1 and stim-exhausted clusters, selected genes are annotated. (D) Heatmap of the top 50 most abundant clonotypes found in CD8+ HNSCC TILs (ward.D2 clustering and binary distance function). (E) Stacked barplot showing the frequency of each clone size definition that is only found in the unstimulated sample (Unique to Unstimulated) or was also recovered post-stimulation (shared). Single (x = 1), small (1 < x < =5), medium (5 < x <=10), large (10 < x <=20) and hyperexpanded (20 < x <= 150). Where x = number of cells with exact CDR3 amino acid sequence. (F) Circos plots depicting the clonal overlap between clusters pre- (unstimulated; top arc) and post-stimulation (stimulated; bottom arc). Ribbons are coloured based on their unstimulated origin. Left column shows ribbons which connect to Stim-1 cluster whereas right column highlight ribbons that originate from ISG (top) or GZMK (bottom) clusters. (G) Same as (F) with left plot highlighted to show ribbons connecting with Stim-exhausted ($Stim_{Ex}$) and ribbons in right plot highlighting those that originate from unstimulated T_{Ex}-1 cluster.

Figure 3: ISG cells are poorly transcriptionally responsive to TCR stimulation

(A) UMAP projection of Stimulated-1, ISG, and GZMK clusters both from unstimulated and stimulated datasets. (B) UMAP projection highlighting TCR clones uniquely found within unstimulated ISG cluster (green) or unstimulated GZMK cluster (black). (C) UMAP projection and quantification highlighting the distribution of unique US-ISG clones post-stimulation. Barplots quantify the frequency of cells post-stimulation. (D) same as (C) but for US-GZMK clones post-stimulation. (E) Pseudotime trajectory inference calculated using Slingshot, demonstrating potential progression of cells from an ISG state via GZMK through to Stim-1 phenotype.

Figure 4: ISG cells are enriched for a type I interferon signature and are associated with reduced transcriptional

(A) Heatmap showing the Top up-regulated DEGs (> 0.25 Log2FC) identified in ISG cluster. (B) Heatmap showing top 10 DEGs identified in ISG cluster. (C) Violin plots of UCell scores for a type I interferon (top) or a type II interferon (bottom) gene signatures. (D) Gene ontology analysis for the top Up-regulated (left) and down-regulated (right) biological processes identified in the ISG cluster.

Figure 5: Cells with a type I interferon signature can be found across various tumor entities and are enriched within tumor tissue

(A) UMAP coordinates of CD8+ T-cells in a pan-cancer dataset overlaid with UCell score for ISG signature. (B) Boxplot showing ISG cluster frequency per donor across normal and tumor tissue samples. (C) Boxplot showing ISG cluster frequency within tumor samples per donor across tumor types within dataset. (D) Circos plots generated using the top 20 interactions for each source (left) or target (right) with ribbons highlighting interactions originating from ISG cluster (left) or terminating in ISG cluster (right), ribbons coloured by source. *p* value calculated using a two-tailed t-test. (n) value indicates the number of unique donors. ns = $p > 0.05$, * = $p < 0.05$, ** = $p < 0.01$, *** = $p < 0.001$, **** $p < 0.0001$.

Supplementary Figure 2: Type I interferon stimulated cells are present in patients with viral infection

(A) Violin plot of UCell score for ISG signature across the CD8+ T-cell clusters within Cillo et al., 2020 dataset. (B) Violin plots of UCell score for type I interferon (left) or type II interferon (right) gene signatures across indicated entities grouped by cells from identified ISG cluster or all remaining cell clusters. (C) UMAP projection of CD8+ T-cells from the COVID-19 Multi-omics Blood Atlas Consortium showing the density of UCell score for ISG signature. (D) Boxplot showing frequency of ISG cluster by disease type per donor. (n) value indicates the

811 number of unique donors. p value calculated using a two-tailed t-test. ns = $p > 0.05$, * = $p < 0.05$,

812 ** = $p < 0.01$, *** = $p < 0.001$, **** $p < 0.0001$.

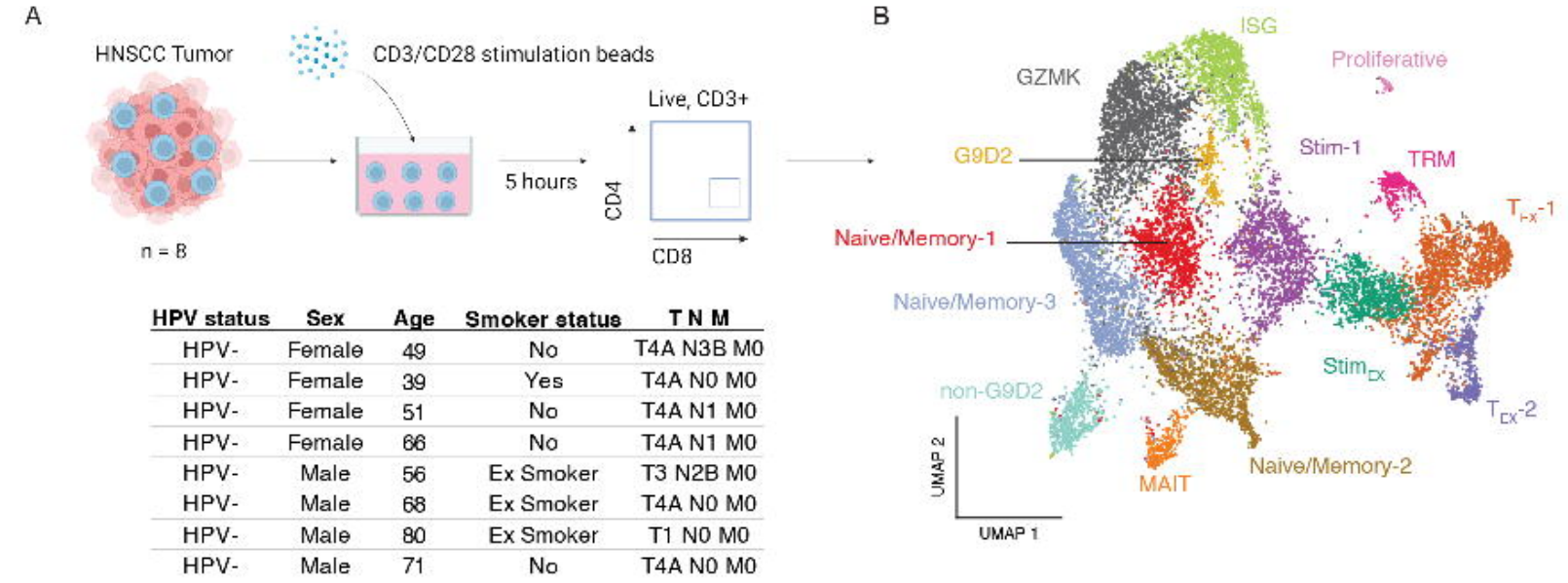

HPV status	Sex	Age	Smoker status	T N M
HPV-	Female	49	No	T4A N3B M0
HPV-	Female	39	Yes	T4A N0 M0
HPV-	Female	51	No	T4A N1 M0
HPV-	Female	66	No	T4A N1 M0
HPV-	Male	56	Ex Smoker	T3 N2B M0
HPV-	Male	68	Ex Smoker	T4A N0 M0
HPV-	Male	80	Ex Smoker	T1 N0 M0
HPV-	Male	71	No	T4A N0 M0

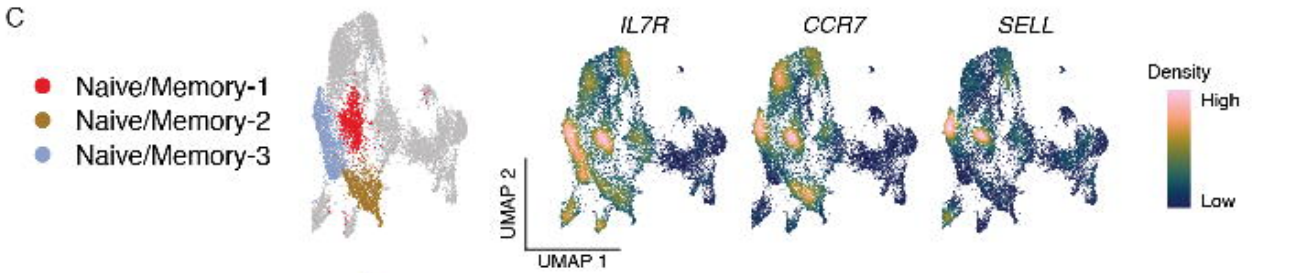

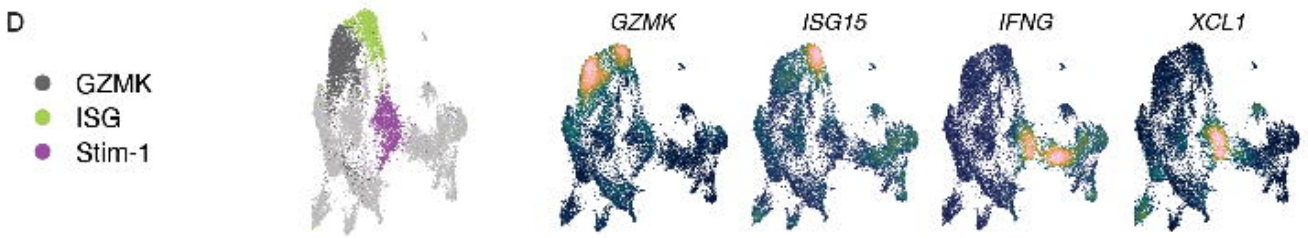

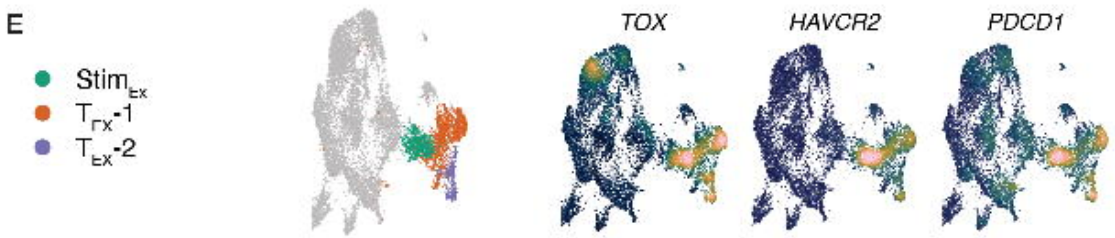

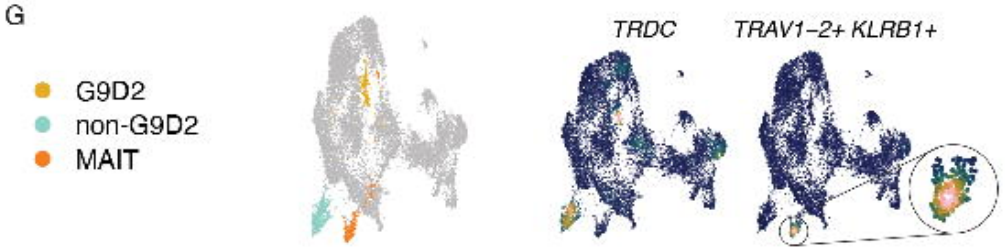

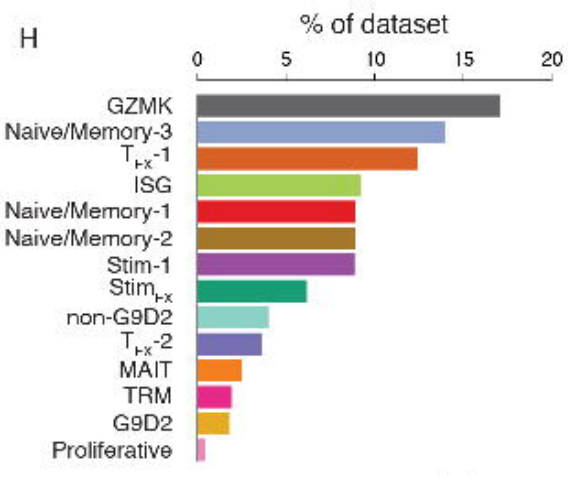

Figure 1

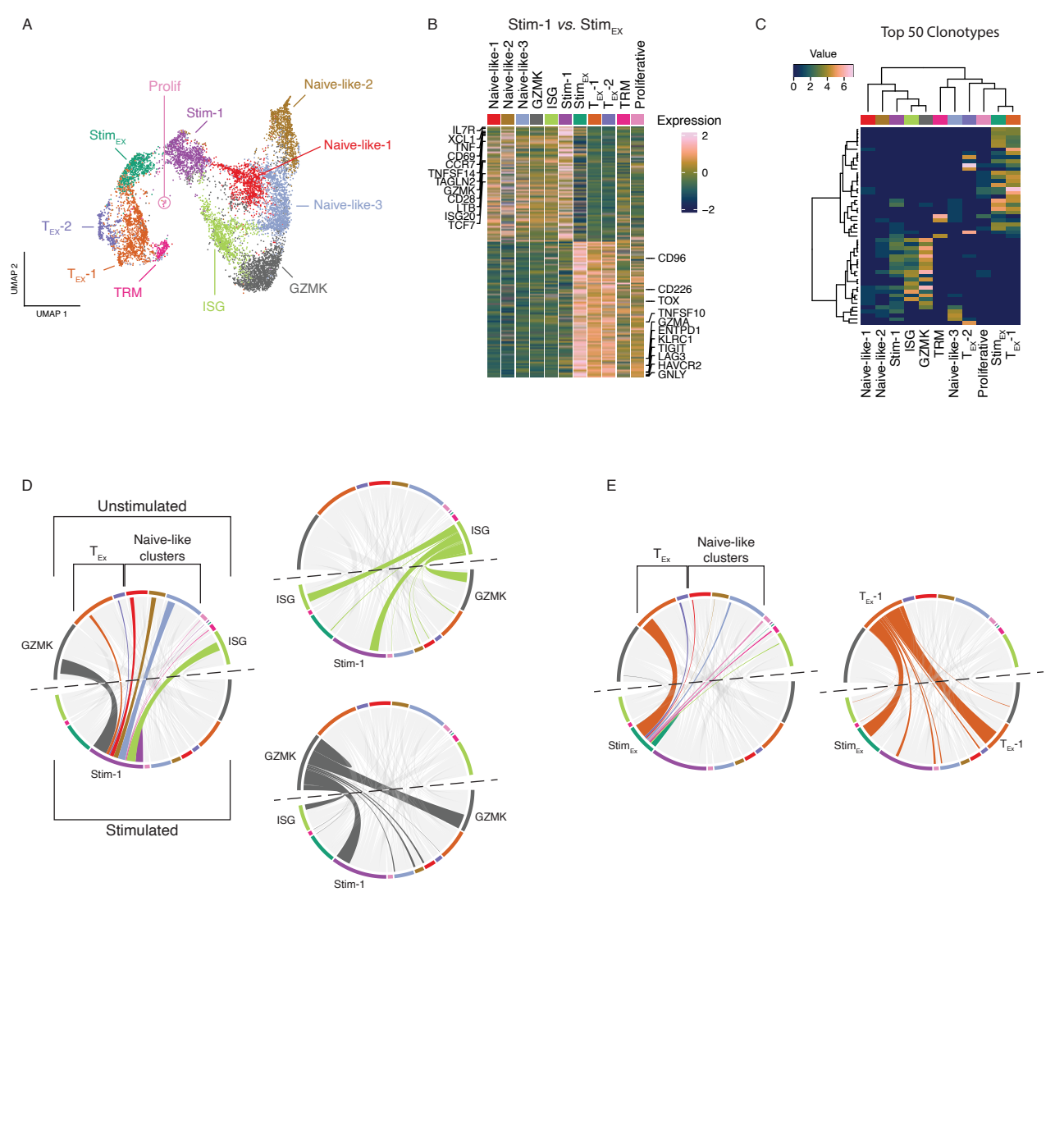
A
Prolif
Stim-1
Stim$_{EX}$
Naive-like-2
Naive-like-1
Naive-like-3
T$_{EX}$-2
T$_{EX}$-1
TRM
ISG
GZMK
UMAP 2
UMAP 1
B
Stim-1 vs. Stim$_{EX}$
Naive-like-1
Naive-like-2
Naive-like-3
GZMK
ISG
Stim-1
Stim$_{EX}$
T$_{EX}$-1
T$_{EX}$-2
TRM
Proliferative
Expression
2
0
−2
IL7R
XCL1
TNF
CD69
CCR7
TNFSF14
TAGLN2
GZMK
CD28
LTB
ISG20
TCF7
CD96
CD226
TOX
TNFSF10
GZMA
ENTPD1
KLRC1
TIGIT
LAG3
HAVCR2
GNLY
C
Top 50 Clonotypes
Value
0 2 4 6
Naive-like-1
Naive-like-2
Stim-1
ISG
GZMK
TRM
Naive-like-3
T$_{EX}$-2
Proliferative
Stim$_{EX}$
T$_{EX}$-1
D
Unstimulated
T$_{Ex}$
Naive-like clusters
GZMK
ISG
Stim-1
Stimulated
ISG
GZMK
Stim-1
GZMK
ISG
Stim-1
E
T$_{Ex}$
Naive-like clusters
Stim$_{Ex}$
T$_{Ex}$-1
Stim$_{Ex}$
T$_{Ex}$-1

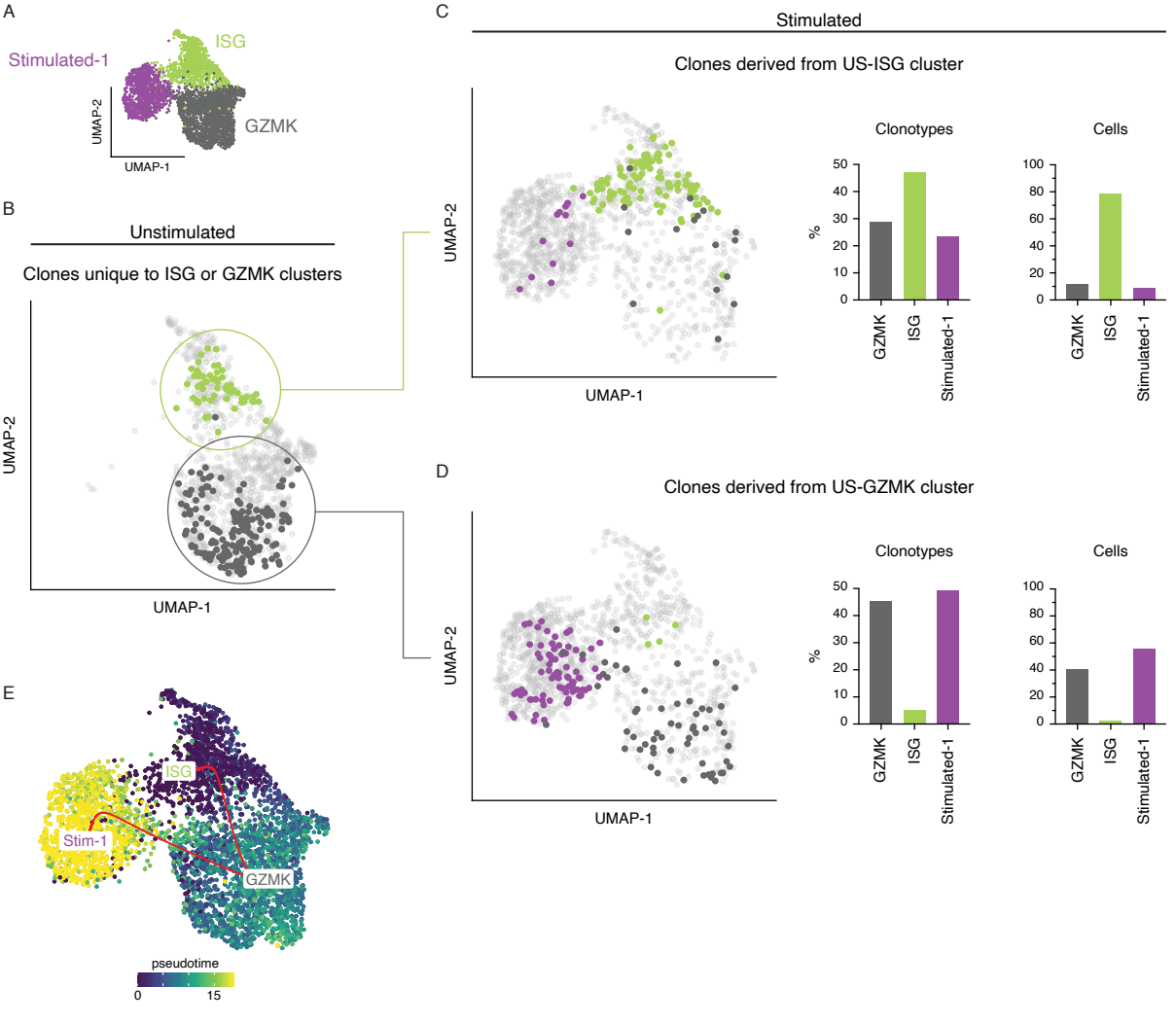
A
Stimulated-1
ISG
GZMK
UMAP-2
UMAP-1
B
Unstimulated
Clones unique to ISG or GZMK clusters
UMAP-2
UMAP-1
C
Stimulated
Clones derived from US-ISG cluster
UMAP-2
UMAP-1
Clonotypes
%
50
40
30
20
10
0
GZMK
ISG
Stimulated-1
Cells
100
80
60
40
20
0
GZMK
ISG
Stimulated-1
D
Clones derived from US-GZMK cluster
UMAP-2
UMAP-1
Clonotypes
%
50
40
30
20
10
0
GZMK
ISG
Stimulated-1
Cells
100
80
60
40
20
0
GZMK
ISG
Stimulated-1
E
ISG
Stim-1
GZMK
pseudotime
0
15

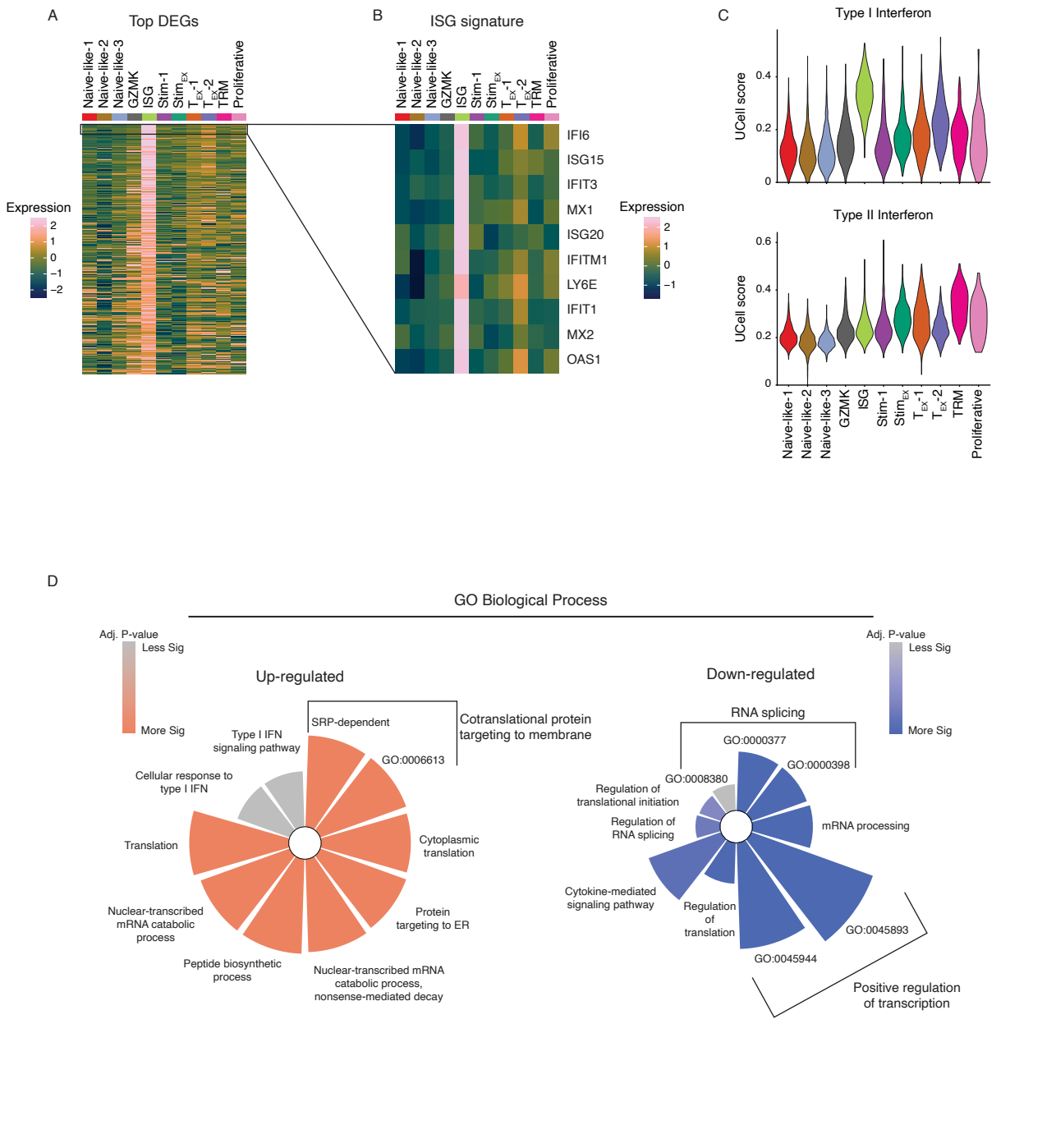
A
Top DEGs
Naive-like-1
Naive-like-2
Naive-like-3
GZMK
ISG
Stim-1
Stim$_{EX}$
T$_{EX}$-1
T$_{EX}$-2
TRM
Proliferative
Expression
2
1
0
−1
−2
B
ISG signature
IFI6
ISG15
IFIT3
MX1
ISG20
IFITM1
LY6E
IFIT1
MX2
OAS1
C
Type I Interferon
UCell score
0
0.2
0.4
Type II Interferon
0.6
D
GO Biological Process
Adj. P-value
Less Sig
More Sig
Up-regulated
SRP-dependent
Cotranslational protein targeting to membrane
Type I IFN signaling pathway
GO:0006613
Cellular response to type I IFN
Translation
Cytoplasmic translation
Nuclear-transcribed mRNA catabolic process
Protein targeting to ER
Peptide biosynthetic process
Nuclear-transcribed mRNA catabolic process, nonsense-mediated decay
Down-regulated
RNA splicing
GO:0000377
GO:0000398
GO:0008380
Regulation of translational initiation
Regulation of RNA splicing
mRNA processing
Cytokine-mediated signaling pathway
Regulation of translation
GO:0045893
GO:0045944
Positive regulation of transcription

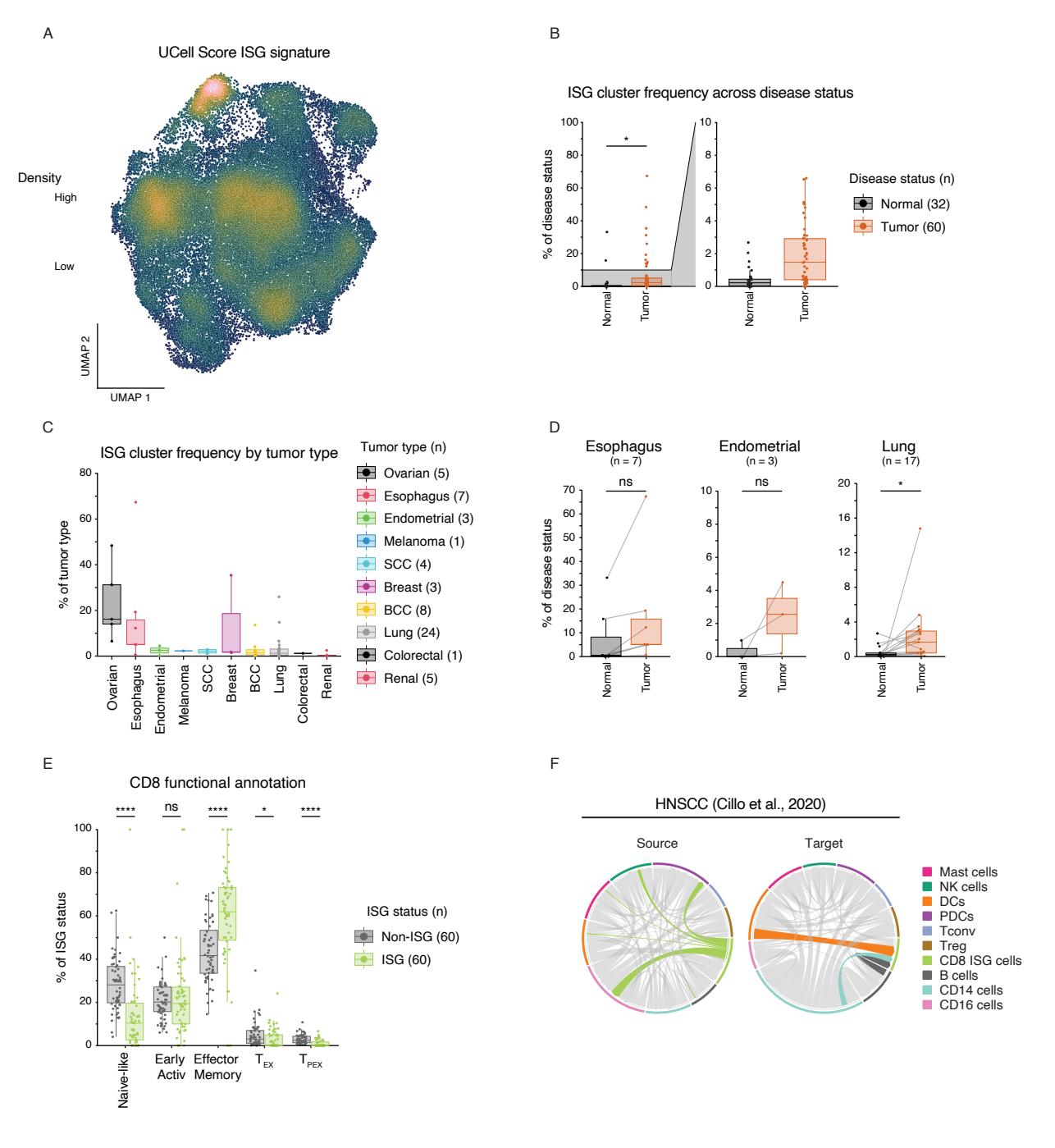
A
UCell Score ISG signature
Density
High
Low
UMAP 2
UMAP 1
B
ISG cluster frequency across disease status
% of disease status
Normal
Tumor
Disease status (n)
Normal (32)
Tumor (60)
C
ISG cluster frequency by tumor type
% of tumor type
Ovarian
Esophagus
Endometrial
Melanoma
SCC
Breast
BCC
Lung
Colorectal
Renal
Tumor type (n)
Ovarian (5)
Esophagus (7)
Endometrial (3)
Melanoma (1)
SCC (4)
Breast (3)
BCC (8)
Lung (24)
Colorectal (1)
Renal (5)
D
Esophagus
(n = 7)
Endometrial
(n = 3)
Lung
(n = 17)
ns
*
% of disease status
Normal
Tumor
E
CD8 functional annotation
% of ISG status
Naive-like
Early Activ
Effector Memory
TEX
TPEX
ISG status (n)
Non-ISG (60)
ISG (60)
F
HNSCC (Cillo et al., 2020)
Source
Target
Mast cells
NK cells
DCs
PDCs
Tconv
Treg
CD8 ISG cells
B cells
CD14 cells
CD16 cells